JOURNAL OF MATERIALS SCIENCE 27 (1992) 1723–1734

Pyrolysis-induced polymetallosiloxane coatings for aluminium substrates

T. SUGAMA
Process Sciences Division, Department of Applied Science, Brookhaven National Laboratory, Upton, NY 11973, USA

C. TAYLOR
University of Virginia, Chemistry Department, McCormick Road, Charlottsville, VA 22901, USA

Inorganic amorphous polymetallosiloxane (PMS) coating films on aluminium substrate were produced through the polycondensation–pyrolysis reaction mechanisms of a sol-precursor solution. The precursor solution was formed by HCl-catalysed hydrolysis of a mixture of *N*-[3-(triethoxysilyl)propyl]-4,5-dihydroimidazole (TSPI) and $M(OC_3H_7)_n$, (M = Zr, Ti and Al, $n = 3$ or 4). The TSPI/$Zr(OC_3H_7)_4$ or $Ti(OC_3H_7)_4$ precursor systems formed higher quality thin coating films, compared to the /$Al(OC_3H_7)$ system. This was because of the critical formation of the polyorganosiloxane terminated by end groups containing zirconium and titanium oxides. These end groups were derived by a dechlorinating reaction between the Cl, bonded to the propyl C in organosilane, and the hydroxylated Zr or Ti compounds in the sintering stages of the film production. Good film-forming performance resulted from moderate degrees of cross-linking of metal oxides to polysiloxane chains and of the densification of metal –O–Si linkages in the pyrolysis-induced PMS network. In addition to these factors, the formation of an oxane bond at the interface between PMS and aluminium provided corrosion protection for the aluminium substrate.

1. Introduction

In the previous work [1], the inorganic polytitanosiloxane (PTS) polymers were synthesized by a polycondensation–pyrolysis reaction processes of sol-precursor solution systems consisting of monomeric organosilanes, $Ti(OC_2H_5)_4$, methanol, water and hydrochloric acid. These PTS polymers were investigated for applicability as corrosion-resistant inorganic polymer coatings for aluminium substrates. A simple dip-coating method was used to deposit the sol-precursor solution layers on the substrates in this investigation. The precursor layer was converted into a sintered coating film by pre-heating in air at 100 °C, and then annealing at 300 °C to form the pyrolysed PTS film. Simple dip-coating technology, a practical application method, offered the following two major advantages: (1) the possibility of placing high-temperature-performing inorganic polymeric coatings on low melting point metal substrates, and (2) the ability to coat substrates with a large surface area by a simple, inexpensive, and efficient method which is compatible with a large-scale, integrated, continuous process run at relatively low temperatures of less than 400 °C. On the other hand, a serious disadvantage is the shrinkage of PTS films caused primarily by the release of carbonaceous species during the annealing processes. This led to the development of stress cracks and pits, thereby resulting in poor protection behaviour by the coatings.

Although the cross-linking ability of the hydroxylated Ti compounds, which connect polysiloxane chains, suppresses the development of these cracks, it was found that the degree of the shrinkage depends upon several factors: (1) the species of monomeric organosilane used as a starting material, (2) the organosilane to $Ti(OC_2H_5)_4$ ratio, (3) the densification of Ti–O–Si linkages, and (4) the number and length of the hydrocarbon chains connecting Ti and Si in the sintered polyorganosilane that contains titanium oxide terminated and substituted end groups. The most effective organosilane precursor for forming PTS coating films containing fewer stress microcracks, was *N*-[3-(triethoxysilyl)propyl]-4,5-dihydroimidazole (TSPI). Thick PTS coatings (thickness, > 10 μm) derived from the appropriate ratio of TSPI/$Ti(OC_2H_5)_4$ displayed good corrosion protection for aluminium upon exposure to NaCl solutions.

Detailed studies regarding the hydrolysis activity of the HCl catalyst which plays an important role in forming the metal oxide–cross-linked polysiloxane networks and in altering the conformation over the temperature range 100–400 °C for the TSPI–titanium alkoxide precursor systems, have not yet been performed. Our research focused on the use of other metal alkoxide species such as $Al(OR)_3$ and $ZR(OR)_4$, ($R = C_3H_7$). In addition, the fabrication of thin film (thickness < 1 μm), which may form a microcrack-

0022–2461

free coatings, because of lower rates of volatility and pyrolysis, was also considered.

Accordingly, the objectives in the present study concerned essentially two research areas. One was to study the thermal behaviour, polycondensation–pyrolysis reaction mechanisms, and the reaction products of the sintered TSPI–metal alkoxide systems. In the second, the surface and interface characteristics of sol-derived thin films as a corrosion-protective coatings on aluminium substrates were evaluated.

2. Experimental procedure

2.1. Materials

The *N*-[3-(triethoxysilyl)propyl]-4,5,-dihydroimidazole (TSPI), was used as a network-forming monomeric organoalkoxysilane. The metal alkoxides employed as cross-linking agent were aluminium, titanium(IV), and zirconium(IV) isopropoxides.

The film-forming mother liquor, which served as the precursor solution, was prepared by incorporating the TSPI–$M(OC_3H_7)_n$, (M = Al, Ti and Zr, $n = 3$ or 4) mixture into a methyl alcohol/water mixing medium containing an appropriate amount of HCl. In order to produce a clear precursor solution, it was very important to add the HCl, as a hydrolysis accelerator, to the blending material, thereby forming a uniform coating film on the metal substrates. The mix compositions for the precursor solution systems used in this study are given in Table I.

The metal substrate used in the experiments was 2024-T3 clad Al sheet containing the following chemical constituents: 92 wt % Al, 0.5 wt % Si, 0.5 wt % Fe, 4.5 wt % Cu, 0.5 wt % Mn, 1.5 wt % Mg, 0.1 wt % Cr, 0.25 wt % Zn, and 0.15 wt % others.

The oxide etching of the Al was carried out in accordance with a well-known commercial sequence called the Forest Products Laboratory (FPL) process [2]. As the first step in the preparation, the surfaces were wiped with acetone-soaked tissues to remove any organic contamination. They were then immersed in chromic–sulphuric acid ($Na_2Cr_2O_7 \cdot 2H_2O : H_2SO_4$: water = 4:23:73 by weight) for 10 min at 80 °C. After etching, the fresh oxide surfaces were washed with deionized water at 30 °C for 5 min, and subsequently dried for 15 min at 50 °C.

Coating of the Al surfaces using the sol system was performed in accordance with the following sequence. The FPL-etched Al substrate was dipped into the precursor solution at ambient temperature. The substrate was then withdrawn slowly from the soaking bath, after which the substrate was preheated in an oven for 20 h at a temperature of 150 °C to yield a sintered coating. The samples were subsequently annealed for 30 min at 350 °C.

2.2. Measurements

The combined techniques of thermogravimetric analysis (TGA), infrared (IR), X-ray powder diffraction (XRD), and X-ray photoelectron spectroscopy (XPS) were used to obtain fundamental data regarding the condensational and pyrolytic changes in conformation, surface and interface chemical components and states, as well as the degree of network cross-linking for the metal alkoxide-modified organosilane polymers at temperatures up to 350 °C.

The surface microstructure and elements of the films after deposition on the Al substrate were observed using scanning electron microscopy (SEM) in conjunction with energy-dispersive X-ray (EDX) analysis.

The electrochemical testing for data on corrosion was performed with an EG&G Princeton Applied Research Model 362-1 Corrosion Measurement System. The electrolyte was a 0.5 M sodium chloride solution made from distilled water and reagent grade salt. The specimen was mounted in a holder and then inserted into a EG&G Model K47 electrochemical cell. The tests were conducted in an aerated 0.5 M NaCl solution at 25 °C, on an exposed surface area of the 1.0 cm^2. The polarization curves containing the cathodic and anodic regions were measured at a scan rate of 0.5 $mV\,s^{-1}$ in the corrosion potential range of -1.2 to -0.3 V.

3. Results and discussion

3.1. Characteristics of sintered organometallicsilane compounds

Before assessing the properties of polymetallosiloxane (PMS) coating films deposited on Al substrates, the thermal and chemical characteristics of the metal alkoxide-modified organosilane compounds were explored using TGA, IR, and XRD techniques. The specific areas of study were the thermal decomposition process, phase-related transitions, pyrolytic changes and rearrangements in conformation, and the crystallization of the sol–gel derived organometallicsilane compounds.

TABLE I Compositions of clear precursor solutions used in various $M(OC_3H_7)_n$-modified TSPI systems. (M = Zr, Ti, Al, $n = 3$ or 4)

TSPI/$M(OC_3H_7)_n$ (wt ratio)	TSPI (wt %)	$Zr(OC_3H_7)_4$ (wt %)	$Ti(OC_3H_7)_4$ (wt %)	$Al(OC_3H_7)_3$ (wt %)	CH_3OH (wt %)	Water (wt %)	HCl (wt %)/TSPI + $M(OC_3H_7)_{4\text{ or }3}$
100/0	50	–	–	–	30	20	12
70/30	35	15	–	–	30	20	20
50/50	25	25	–	–	30	20	30
70/30	35	–	15	–	30	20	15
50/50	25	–	25	–	30	20	25
70/30	35	–	–	15	30	20	40
50/50	25	–	–	25	30	20	50

The aim in this broad exploration was to understand the thermal decomposition process and the transition of the sintered organometallicsilane to its inorganic polymer phase by pyrolysis in an air environment. From the mix compositions given in Table I, 150 °C sintered powder samples with 100/0 and 50/50 TSPI/$M(OC_3H_7)_{4\text{ or }3}$ weight ratios were selected. Their TGA curves are depicted in Fig. 1. The onset temperatures of decomposition were obtained by finding the intersection point of the two linear extrapolations. As one can see, the onset temperature depends upon the species of metal alkoxide reagent added to the TSPI. The beginning of thermal decomposition for all of the samples, with the exception of the $Al(OH_3H_7)_3$–TSPI system, is likely to occur over the temperature range 300–350 °C. Decomposition of the TSPI/$Al(OC_3H_7)_3$ system started at a lower temperature (200 °C) than the other metal alkoxide systems. The weight loss curve of bulk TSPI exhibited the two step decomposition process; the first step occurring at a temperature between 350 and 430 °C and the second step ranging from 430–600 °C. The former change might be associated with the liberation of hydrocarbon and chemisorbed water; the latter may be caused by the removal of excess carbon in the samples. Beyond the annealing temperature of 600 °C, the curve levels off, implying that the conversion into inorganic phases is essentially complete. Although the curve shapes of the TSPI/$M(OC_3H_7)_{4\text{ or }3}$ systems are unlike that of the bulk TSPI, the final transition temperature to the inorganic phase was almost the same as the bulk TSPI. When compared to the weight loss (approximately 42%) of TSPI at 600 °C, less of a weight loss was observed for the $Ti(OC_3H_7)_4$ system, whereas the $Al(OC_3H_7)_3$ system had considerable mass loss, approximately 68%. This large weight loss caused by the pyrolysis could be associated with an enhanced degree of shrinkage of the precursor coating films that results in cracking and delamination of the films from the substrates.

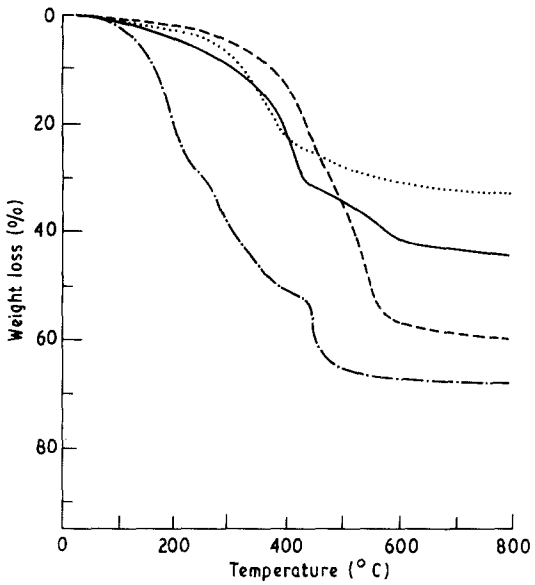

Figure 1 TGA curves of metal isopropoxide-modified and unmodified TSPI powders after sintering at 150 °C. (——) TSPI, (– – –) Zr$(OC_3H_7)_4$–TSPI, (· · ·) $Ti(OC_3H_7)_4$–TSPI, (—·—) $Al(OC_3H_7)_3$–TSPI.

Based upon TGA data, the pyrolytic changes and rearrangements in conformation at 350 °C were studied with IR. Fig. 2 shows the IR absorption spectra for 150 °C-preheated powder samples of bulk TSPI and the TSPI/metal alkoxide, 50/50 ratio samples. The IR analyses were conducted using the KBr method which incorporates the powder samples of 2–3 mg into KBr pellets of approximately 200 mg. For the metal alkoxide–TSPI samples and the TSPI bulk sample, the various absorption peaks and their assignments are shown in Fig. 2 and Table II. In the TSPI bulk sample (Fig. 2a), the shoulder peak due to the superposition of physically absorbed water and hydrogen-bonded O–H stretching in silanol Si–OH groups is located at 3450 cm^{-1} [3]. Because no N–H bond exists in the monomeric TSPI used as a starting material, the peak assignment at 3240 cm^{-1} seems to reveal a newly developed N–H stretching mode in the dihydroimidazole [4]. The bands around 2930 and 2880 cm^{-1} are attributed to absorptions due to the C–H stretching mode in the methylene chains and dihydroimidazole rings. The C–H bending mode peaks appear at 1435 and 1395 cm^{-1}. An intense absorption peak, observed at 1655 cm^{-1}, is ascribed to the imine, $\diagdown$C=N–, stretching vibration in the five-membered dihydroimidazole rings [5]. Five-membered heterocycles commonly have two other fundamental ring stretching bands at frequencies ranging from 1670–1400 cm^{-1} [6]. Thus, the weak peak near 1525 cm^{-1} could reflect on the ring-stretching modes. The other peak corresponding to the heterocyclic rings may be masked by strong C–H absorption in the vicinity of 1430 cm^{-1}. The pronounced peak at 1135 cm^{-1} verifies the existence of the stretching mode of the Si–O–C bond in the Si-joined alkoxy groups [7]. As is well known [3], the peaks at 1035 and 775 cm^{-1} are associated with the stretching of Si–O–Si and the bending of Si–O–Si bonds, respectively. These bonds in the polymeric organosilane are formed by the condensation reactions between neighbouring silanol functions. The new peak developed at 695 cm^{-1} can be assigned to the C–Cl stretching band in the chlorinated compounds [8]. The development of this C–Cl band can be

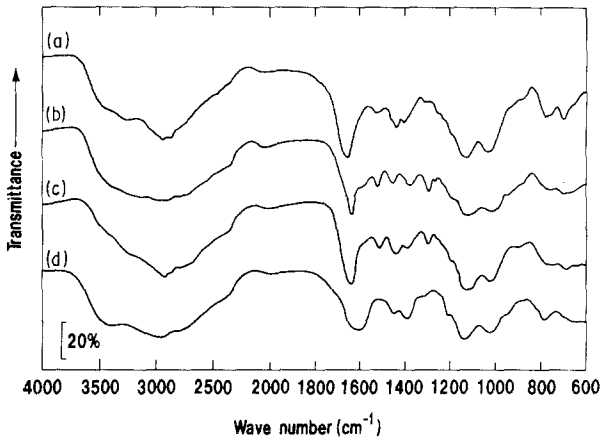

Figure 2 IR adsorption spectra for 150 °C-sintered powder samples having 100/0 and 50/50 TSPI/$M(OC_3H_7)_{4\text{ or }3}$ ratios; (a) TSPI, (b) TSPI/$Zr(OC_3H_7)_4$, (c) TSPI/$Ti(OC_3H_7)_4$, and (d) TSPI/$Al(OC_3H_7)_3$.

explained if the emergence of the N–H peak at 3240 cm^{-1} is taken into consideration. Because the imidazole group in TSPI acts as a strong base by accepting a proton [9], the nucleophillic attack of H^+ to the dihydroimidazole N bonded to the propyl group in the HCl media leads to the cleavage of the $N–CH_2$ linkage [10]. Then this bond breakage forms the imidazoline as derivative of dihydroimidazole,

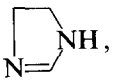

, and polymeric organosilane containing Cl-substituted end groups. This HCl-catalysed hydrolysis-polycondensation reaction will occur according to the following sequence

(1)

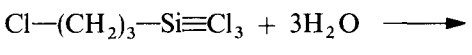

(2)

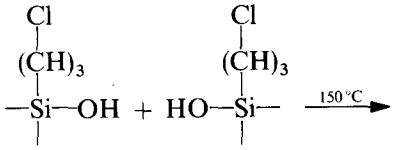

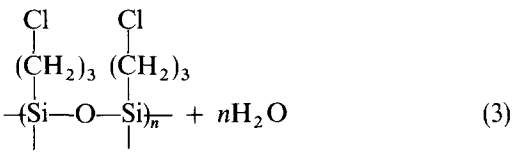

(3)

On the basis of the information, the spectral features of the metal alkoxide-modified TSPI samples were investigated to identify the reaction products of TSPI with metal alkoxides at a low temperature, 150 °C. Compared with the spectrum for bulk TSPI, characteristics noted for the $Zr(OC_3H_7)_4$– and $Ti(OC_3H_7)_4$-systems spectra (Fig. 2b and c) are as follows: (1) the appearance of a notable peak near 1300 cm^{-1} which corresponds to metal (Zr and Ti) –O–C linkages [11], (2) the loss in C–Cl peak intensity at 695 cm^{-1}, and (3) no remarkable peak present around 950 cm^{-1} which would be attributable to the Zr– or Ti–O–Si linkages [3, 12] in the PMS formed. As a result, it is believed that the hydroxyl groups derived from the HCl-catalysed hydrolysis of $Zr(OC_3H_7)_4$ and $Ti(OC_3H_7)_4$, react preferentially with the Cl in Cl-substituted end groups in the silane compound, rather than the silanol groups which are formed by hydrolysis of the ethoxysilyl groups in the TSPI. The proposed reaction mechanism for this is shown below

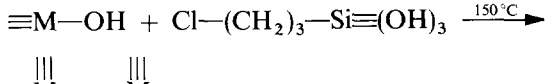

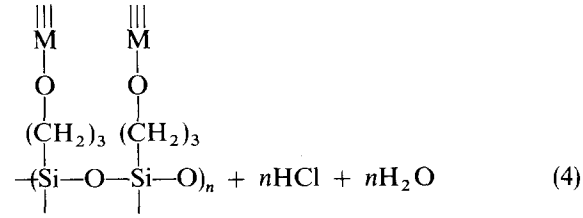

(4)

where M = Zr or Ti.

At 150 °C, the two major components, polymeric organosilane containing oxygen-bridged metal compounds and isolated dehydroimidazole derivative, appear to be present in the pre-heated materials.

To support the proposed reaction mechanism, the absorbance ratios between the M–O–C peak at 1300 cm^{-1} and the C–Cl peak at 695 cm^{-1} were computed as a function of the TSPI/$M(OC_3H_7)_4$ ratio. As expected, the resultant data (see Fig. 3) indicate that the absorbance ratios increase with an increase in the proportion of $M(OC_3H_7)_4$. This, thereby, implies that the reaction of the halide with the OH in the hydroxylated metals favours the elimination of hydrogen chloride. The formation of Cl-terminated end groups plays an important role in creating the M–O–C linkages.

On the other hand, the introduction of $Al(OC_3H_7)_3$ reagent into the TSPI results in many different features being present in the spectrum (Fig. 2d). Specifically, no peaks from the N–H stretching and ring-stretching modes in the dihydroimidazole derivative at 3240 and 1525 cm^{-1}, the M–O–C linkage band at 1300 cm^{-1} and the C–Cl bond peak at 695 cm^{-1}, were found. However, two new absorption frequencies around 1590 and 945 cm^{-1} did emerge. Because dihydroimidazole ring stretching in monomeric TSPI is discernible from a strong peak in the vicinity of 1610 cm^{-1} (not shown), the first of the new peaks may reveal the presence of the original dihydroimidazole attached to the propyl C of TSPI. The formation of Al–O–Si linkages possibly explains the new absorption band at 945 cm^{-1} [13, 14]. Therefore, compared to the $Zr(OC_3H_7)_4$– and $Ti(OC_3H_7)_3$–TSPI systems, a different reaction process occurs in the $Al(OC_3H_7)_3$–TSPI system. Questions as to why this system does not produce heterocyclic derivatives and the Cl-substituted end groups still remain. It is evident that polymeric organoaluminosilane network structures containing Al–O–Si linkages do form at 150 °C. The conformation of this hypothetical reaction product may be as follows:

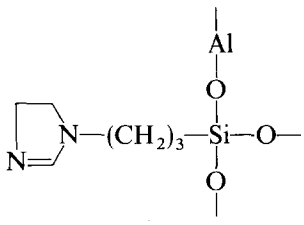

(I)

The IR studies were further extended in an attempt to understand and clarify the pyrolytic conformation changes in inorganic PMS produced by annealing in air at high temperatures. All of the 150 °C pre-heated samples were heated for 12 h in air at 350 °C. Fig. 4

TABLE II Summary of the assignments of IR absorption detected in the spectra of bulk TSPI sample at 150 °C

Wave numbers (cm^{-1})	Vibration[a]	Absorbing species
3450	νOH	H–O–Si and H_2O
3240	νNH	H–N in dihydroimidazole derivative
2930	νCH	$-CH_2-$ and dihydroimidazole derivative
2880	νCH	$-CH_2-$ and dihydroimidazole derivative
1655	νCN	–C=N– in dihydroimidazole derivative
1525	ν ring	in dihydroimidazole derivative
1435	δCH and ν ring	$-CH_2-$ and dihydroimidazole derivative
1395	δCH	$-CH_2-$ and dihydroimidazole derivative
1135	νSi–O–C	$Si-O-C_2H_5$
1035	νSi–O–Si	Si–O–Si
775	δSi–O–Si	Si–O–Si
695	νC–Cl	$Cl-CH_2-$

[a] ν denotes stretching vibration, δ denotes bending vibration.

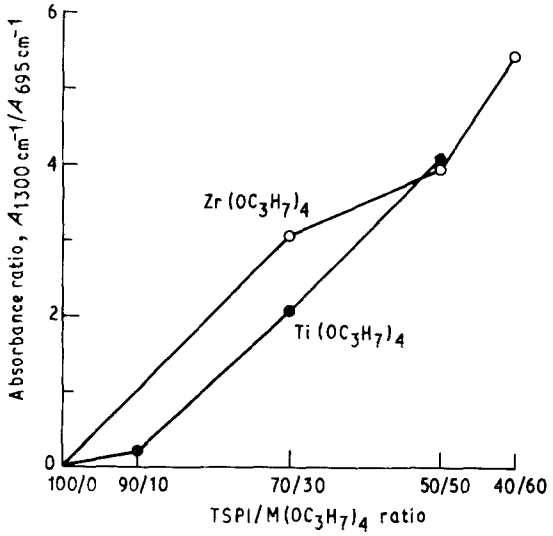

Figure 3 Variations in absorbance ratio of M–O–C at 1300 cm^{-1} to C–Cl at 695 cm^{-1} as a function of TSPI/$M(OC_3H_7)_4$ ratios.

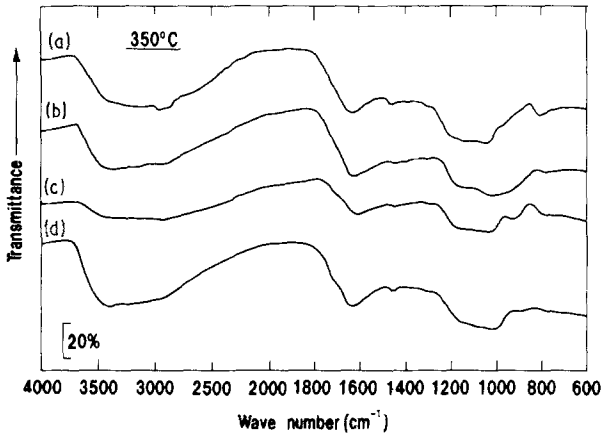

Figure 4 IR spectra for 350 °C-annealed 100/0 and 50/50 TSPI/$M(OC_3H_7)_{4\ or\ 3}$ systems; (a) TSPI, (b) TSPI/$Zr(OC_3H_7)_4$, (c) TSPI/$Ti(OC_3H_7)_4$, and (d) TSPI/$Al(OC_3H_7)_3$.

illustrates the IR spectra for the 350 °C annealed sample series. The bulk TSPI sample spectrum (Fig. 4a) changed markedly, compared with the 150 °C treated sample spectra. These changes are as follows: (1) a considerable loss in intensity of the peaks at 2930, 2880, 1435 and 1395 cm^{-1}, (2) a slight shift of the >C=N– band at 1655 cm^{-1} toward lower wave numbers (1620 cm^{-1}), (3) a decrease in intensity of the peak around 1135 cm^{-1} corresponding to a decrease in $Si-CH_2-$ bonds, and (4) a disappearance of the C–Cl peak at 697 cm^{-1}. Changes (1), (3) and (4) result directly from the elimination of a large amount of carbonaceous groups such as CH_2O and CH_3CHO from the polymeric organosilane networks. The absorption band near 3400 cm^{-1} and a weak band around 1450 cm^{-1}, are due to the superposition of ring stretching and H–O–H bending vibrations. Thus, around 350 °C the polymeric organosilane is believed to be pyrolytic converted into the inorganic polysiloxane network. Nevertheless, some residual imidazole derivative still remains in the polysiloxane network.

Attention was then focused on the spectra for the TSPI/$Zr(OC_3H_7)_4$ (Fig. 4b) and TSPI/$Ti(OC_3H_7)_4$ (Fig. 4c) systems. The depicted spectrum features of annealed samples were characterized by the development of new peaks at 950 cm^{-1} (b) and 930 cm^{-1} (c). These absorption bands signify the formation of Zr–O–Si or Ti–O–Si linkages, respectively. The predominance of the Si–O–Si band around 1020 cm^{-1}, proves that the inorganic PMS structures can be formed at 350 °C through the pyrolytic *in situ* transformation processes shown below

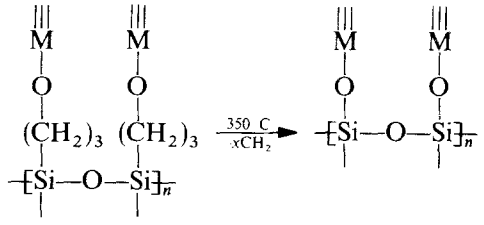

(5)

Where M = Zr or Ti. Under annealing conditions, these pyrolytic conformation changes occur with the elimination of numerous organic groups. Once the organopolysilane–inorganic PMS transition is completed, the Zr and Ti metal oxides located in the networks act as cross-linking agents which connect the polysiloxane chains.

In contrast, the spectrum for the postannealed TSPI/$Al(O_3H_7)_3$ system indicated the shift in the Si–O–Si band at 1035 cm^{-1} to a lower position of 1000 cm^{-1} and the disappearance of the 950 cm^{-1} peak corresponding to the Al–O–Si linkages. The shifting and disappearance of these peaks render the thermal decompositions of 150 °C-formed organo-polyaluminosilane as a means of the bond breakages of Al–O–Si linkages. This strongly suggests that the Al–O–Si bond-based network structures, which are formed readily at a low temperature of 150 °C, are vulnerable to pyrolysis. However, conformation of the pyrolytically assembled PMS, which is represented by the metal oxide cross-linked polysiloxane networks, is responsible for the development of high-temperature-performance inorganic polymer structures.

In addition to TGA and IR analyses, an XRD study was considered necessary to determine whether the pyrolysed materials had crystallized. Fig. 5 represents the XRD patterns of the 350 °C annealed metal alkoxide–TSPI systems, over the diffraction range 0.444–0.182 nm. For the $Zr(OC_3H_7)_4$ (a) and $Al(OC_3H_7)_3$ (b) systems, no spacing lines were detected over this diffraction range. Hence, this indicates that the PMS in these systems is essentially amorphous. In contrast, the reflections at 0.353, 0.236 and 0.190 nm for the TSPI/$Ti(OC_3H_7)_4$ system are attributable to the presence of a certain amount of anatase, TiO_2, crystalline particles in the amorphous polytitanosiloxane layers.

3.2. Characteristics of PMS coating films

On the basis of the above findings, the investigations were focused on understanding the physico-chemical factors governing the formation and fabrication of high-quality PMS coating films. Uniformity and continuity were studied using surface and interface analytical tools such as SEM–EDX, and XPS. As described earlier in Section 1, thin PMS films with a thickness of up to 0.5 μm are of particular interest to this study. To obtain a thin coating film, 20 g of the original precursor sol solution (shown in Table I) was diluted with 80 g deionized water. First the FPL-etched Al substrate was dipped into the diluted film-forming precursor solution, and then sintered in an oven at 150 °C for 20 h. In order to form the pyrolysis-induced PMS coating films, the 150 °C sintered samples were subsequently annealed for 30 min at 350 °C. The thickness of the PMS film deposited on the substrate was determined using a surface profile measuring system. The average thickness of the films derived from the precursor solution consisting of 100/0, 70/30, and 50/50 TSPI/$M(OC_3H_7)_{4\text{ or }3}$ ratios, ranged approximately, from 0.2–0.4 μm.

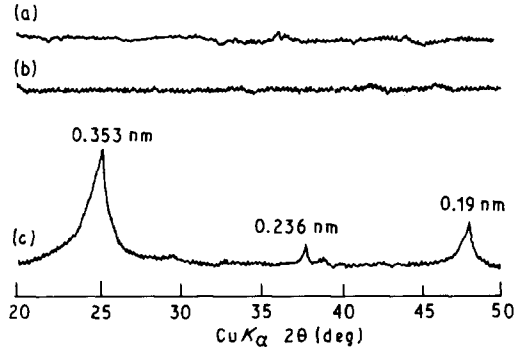

Figure 5 XRD tracings for 350 °C-annealed 50/50 (a) TSPI/$Zr(OC_3H_7)_4$, (b) TSPI/$Al(OC_3H_7)_3$ and (c) TSPI/$Ti(OC_3H_7)_4$ systems.

Fig. 6 shows a scanning electron micrograph for the metal oxide–uncross-linked polysiloxane (PS) originating from the 100/0 ratio precursor. The surface microstructure of this pyrolysed film reveals a large number of pits and microcracks. The EDX spectrum (not shown) accompanying the SEM image indicated Si to be a principle component of the film, but Cl was not detected in the film. Thus, the HCl which was used as a hydrolytic catalyst of TSPI was probably eliminated from the sintered precursor films during the pyrolysis at 350 °C. Therefore, possible attack to the Al substrate by corrosive dissociated Cl ions was disregarded. Although some microcracks were present, the polyzirconosiloxane (PZS) film derived from the 70/30 TSPI/$Zr(OC_3H_7)_4$ ratio precursor (Fig. 7a), exhibited far better coating features and no pits. EDX quantitative evaluation of this film indicated that no Cl was present and that the Zr to Si intensity count ratio was 0.17. Compared with the 70/30 ratio sample, the 50/50 ratio-derived PZS film had numerous microcracks (Fig. 7b). Hence, the incorporation of an excessive amount of $Zr(OC_3H_7)_4$ in TSPI leads to the generation of stresses within the film brought about by differences in the thermal expansion and/or the differential shrinkage between the film and substrate during pyrolysis.

In the case of the polyaluminosiloxane (PAS) derived from TSPI–$Al(OC_3H_7)_3$ systems, SEM images for either 70/30 (Fig. 8a) or 50/50 (Fig. 8b) ratios indicate film discontinuity and non-uniform features, and partial delamination from the substrate. These

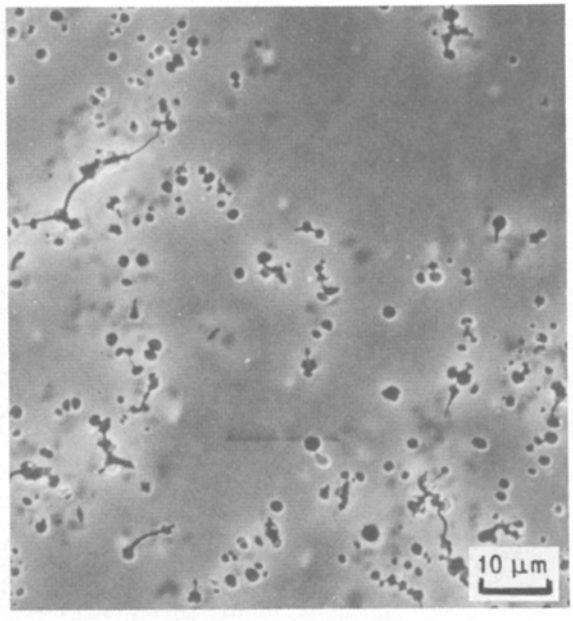

Figure 6 Scanning electron micrograph of PS coating film derived from 100% TSPI at 350 °C.

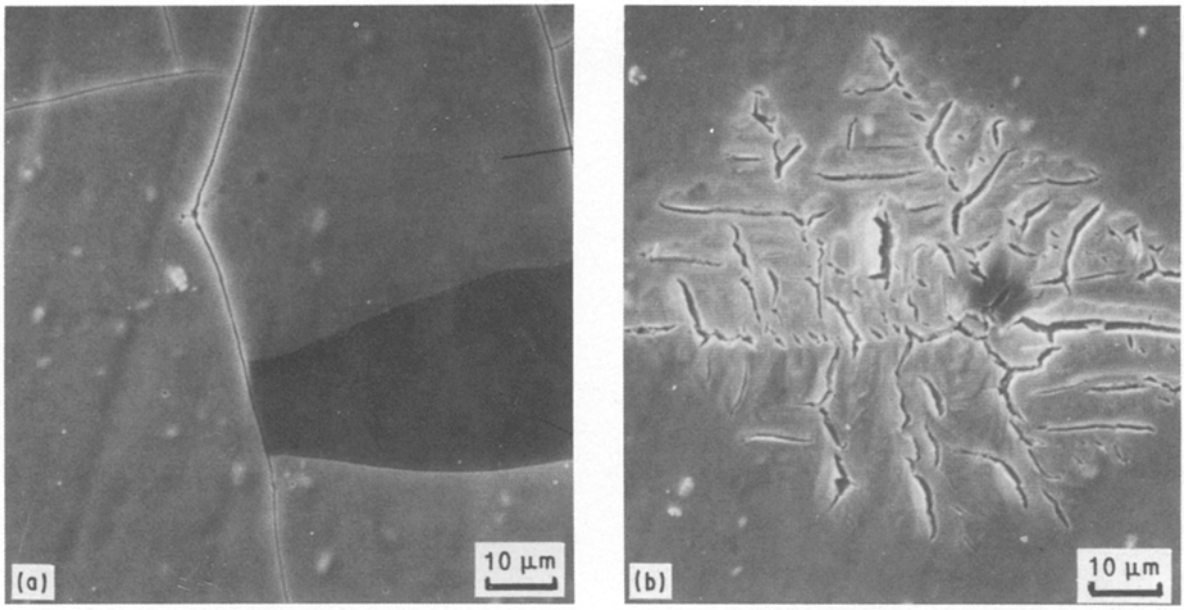

(c)

Element	Intensity (counts/30s)	Intensity ratio/Si
Zr	239	0.17
Si	1407	1.00
Cl	0	0.00

Figure 7 SEM (a, b) images and (c) EDX analysis of PZS coatings formed by annealing at 350 °C (a) 70/30 and (b) 50/50 TSPI/$Zr(OC_3H_7)_4$ ratio precursor films.

undesirable film-forming characteristics, in connection with the results of TGA and IR, are due presumably to great stresses generated at the film–substrate interface caused by the large weight loss and thermal decomposition of the film due to Al–O–Si linkages breaking. The most ideal PMS coating surface consists of a uniform film free of cracks and pits over large dimensions. These characteristics were observed in the 50/50 TSPI/$Ti(OC_3H_7)_4$ ratio (Fig. 9b)-derived polytitanosiloxane (PTS). However, in the 70/30 ratio film, a few microcracks developed (Fig. 9a). It appears that the use of a proper TSPI to $Ti(OC_3H_7)_4$ proportion is one of the important factors leading to the formation of high-quality inorganic PTS amorphous coatings containing crystalline anatase particles.

Further experimental work focused on identifying the chemical components and states at the outermost surface of the various PMS coatings. XPS was used to obtain this information for coatings derived from a 70/30 TSPI/$M(OC_3H_7)_{4\text{ or }3}$ ratio precursor solution. For the scale in all the XPS spectra, the binding energy (BE) was calibrated with the C_{1s} of the principal hydrocarbon-type C peak fixed at 285.0 eV as an internal reference standard. The C_{1s} core level spectrum of the PMS surfaces was not taken into consideration, because the concentration of hydrocarbon impurities on pyrolysis-induced surfaces was negligible compared to the intensity of the signal from the

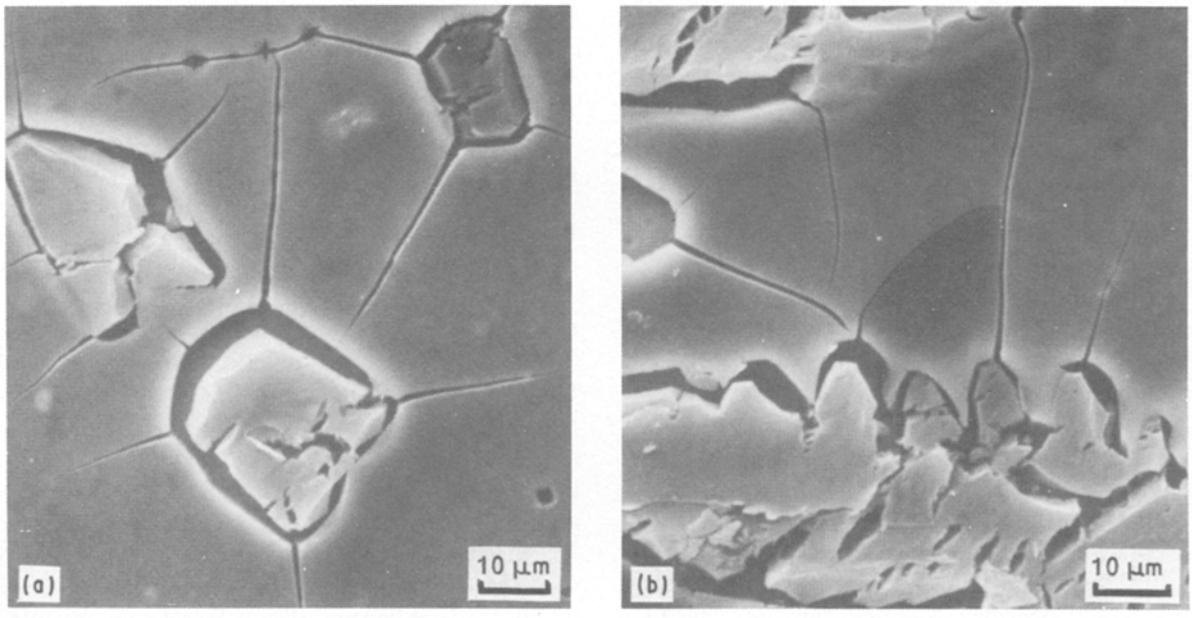

Figure 8 SEM images of 350 °C-pyrolysed (a) 70/30 and (b) 50/50 TSPI/$Al(OC_3H_7)_3$ ratio coating films.

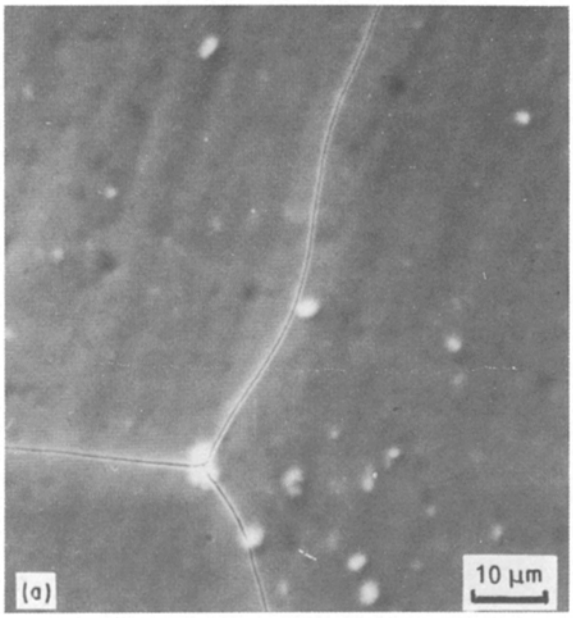

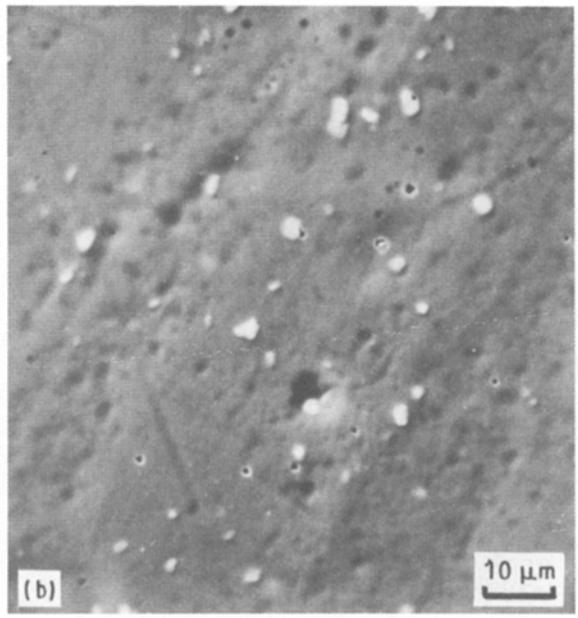

(c)

Element	Intensity (counts/30s)	Intensity ratio/Si
Ti	2692	2.38
Si	1132	1.00
Cl	0	0.00

(d)

Element	Intensity (counts/30s)	Intensity ratio/Si
Ti	3330	7.38
Si	451	1.00
Cl	0	0.00

Figure 9 (a, b) Surface features and (c, d) EDX data of pyrolysis-induced PTS coating films; (a) 70/30 and (b) 50/50 TSPI/Ti $(OC_3H_7)_4$ ratio systems.

unpyrolysed samples. A curve deconvolution technique was employed to find the respective chemical components from the high-resolution spectra of each element, and to determine the relative quantity of a particular chemical state.

The Si_{2p} and O_{1s} core level photoemission spectra for the PS (derived from 100% TSPI), PZS, PTS, and PAS films are shown in Figs 10 and 11, respectively. The Si_{2p} region for the PS coating (Fig. 10a) reveals only a single peak at 102.8 eV, corresponding to the silicon in the siloxane bonds, Si–O–Si [15, 16]. Drastic changes in the position, intensity, and shape of the Si_{2p} peak were induced when zirconium, titanium and aluminium oxides were incorporated in the PS network as cross-linking agents. The Si_{2p} signal for the PZS surface (Fig. 10b) could be resolved into two Gaussian components at 101.6 and 102.8 eV. The former peak as the principal component corresponds to the silicon in the Zr–O–Si linkages [17, 18]; and the latter ascribes the siloxane Si as a minor component. The peak shape of the PTS film (Fig. 10c) is strikingly different from that of the PZS. The peak of siloxane Si emerged at 102.8 eV is of a principal component, while a shoulder peak at 101.6 eV, interpreted as the Si in the Ti–O–Si bonds, is of a minor component. This infers that the extent of cross-linking of titanium oxides in the PTS coating is lower than that of the zirconium oxides in PZS. Peak features similar to those of PZS were observed on the PAS film (Fig. 10d), suggesting that, like PZS, the surface contains a highly densified Al–O–Si network. The O_{1s} spectrum of PS (Fig. 11a) exhibits an asymmetric shape containing a main peak at 532.4 eV originating from the bridging oxygen-bonded to two Si atoms (the siloxane bond). Assuming that the nonbridging oxygens are bonded to one Si, and more likely to one H (the hydroxylated Si) are present at the PS surface, the cause of the shoulder at $\approx$ 529.4 eV can be established. This shoulder, which is about 3.0 eV lower than that of the bridging oxygens in the Si–O–Si, is attributable to nonbridging oxygens [19]. In contrast, O_{1s} spectra for the PMS coatings are characterized by a broad, asymmetric peak which obviously contains at least three components situated at 532.4, 531.5, and $\approx$ 529.4 eV. The major component at 531.5 eV belongs to the metal-bound oxygen in the M–O–Si linkages [20]. The two shoulders at 532.4 and $\approx$ 529.4 eV are presumably due to the bridging oxygens in the Si–O–Si and the nonbridging oxygens in the Si–OH, respectively. The intensity of the nonbridging oxygen peak seems to depend on the species of PMS. The quantitative evaluation of Si–OH groups existing at the outermost surface was carried out by comparing the integrated intensity ratio of oxygen in Si–OH peak at approximately 529.4 eV to oxygen in the M–O–Si peak at approximately 531.5 eV. As a result, the PTS surface indicated the highest ratio of 0.53 (Fig. 11). Because the peak of TiO_2 oxygen appears near 529.4 eV [21, 22], this peak will include contributions from both SiOH and TiO_2 oxygens. Nevertheless, the presence of an appreciable number of polar OH groups at the surface of PMS is very important to adhesion. It is believed that the OH in the hydroxylated Si compound promotes the chemical

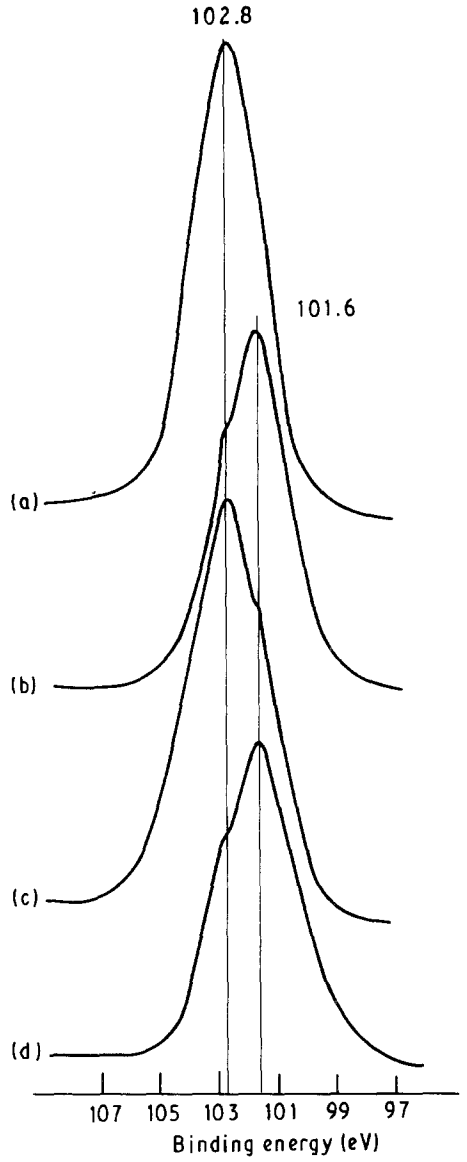

Figure 10 Si 2p spectra originating from (a) PS, (b) PZS, (c) PTS and (d) PAS coating surfaces.

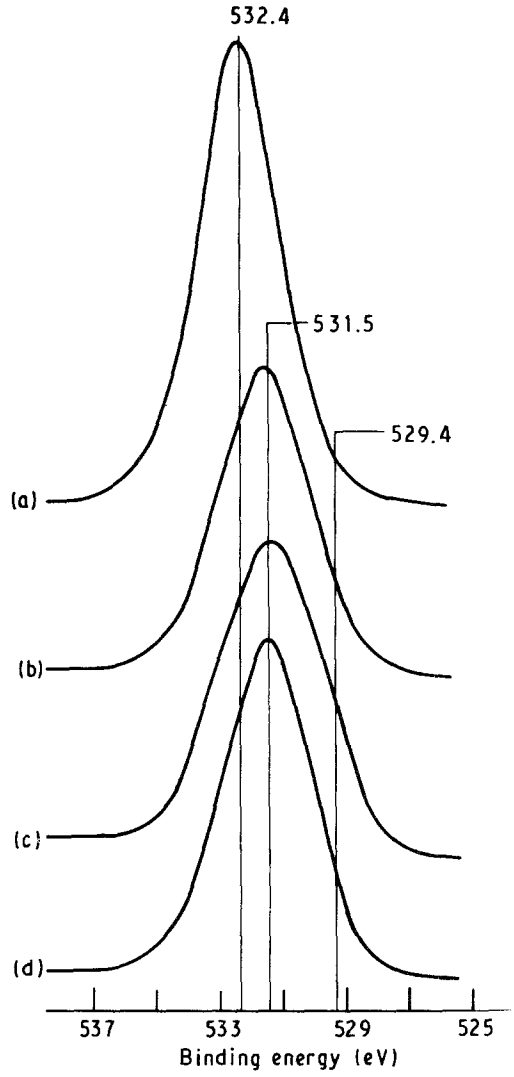

Figure 11 O 1s region of (a) PS, (b) PZS, (c) PTS and (d) PAS. Integrated intensity ratio of O(SiOH)/O(M–O–Si): (b) 0.3, (c) 0.53 and (d) 0.36.

link between the organic and inorganic polymers through covalent or H bonds. Fig. 12 illustrates the Zr 3d and Ti 2p doublet separation spectra for PZS and PTS, respectively, and the Al 2p region for PAS. The $3d_{5/2}$ and the $3d_{3/2}$ lines at 182.3 and 184.2 eV for Zr_{3d} spectrum are assigned to the Zr in the Zr–O–Si linkages. The symmetric peak at 74.1 eV in the Al 2p spectrum corresponds to the Al in the Al–O–Si bonds [17]. For PTS, there are four peaks in the Ti 2p regions. The main $2p_{3/2}$ peak at 458.7 eV and the $2p_{1/2}$ line at 464.5 eV are assigned to the Ti in the Ti–O–Si linkages. The anatase titanium was observed in the $2p_{3/2}$ peak at approximately 459.2 eV and $2p_{1/2}$ peak at approximately 465.1 eV [23].

The adhesive nature at the interface between PMS and the FPL-etched Al substrate is an important factor contributing to a good film-forming behaviour and to subsequent corrosion protection. Therefore, it is worthwhile to assess the bonding structure and mechanism at the PMS–Al interface. For these interface studies, a PTS coating was selected from the other PMS films. The thin PTS films suitable for XPS analyses were fabricated on the etched substrates in accordance with the following procedure: a 0.5% sol-precursor solution in deionized water was deposited over the substrate surfaces by spin-coating at 1000 r.p.m., and then heated for 20 h at 150 °C to produce a sintered film. The pyrolytic conversion of the sintered film into the PTS film was accomplished by annealing for 30 min at 350 °C. Finally, the resulting interfaces were examined using XPS.

The PTS films made by this method were thin enough to permit the photo-emission signal from the underlying Al substrate to be detected. Figs 13 and 14 show the Al 2p and the O 1s core level spectra for the FPL-etched substrate and for the interface between the PTS and the substrate. As is evident from the Al 2p peak at 74.4 eV (Fig. 13a), the main component of the outer surface of Al is aluminium oxide, Al_2O_3 [20]. The Al 2p signal at the PTS–Al interface (Fig. 13b) is composed of two major components at 74.4 and $\approx$ 74.0 eV. The exciting photoemission at 74.4 eV originates from Al_2O_3 aluminium; however, the new line at $\approx$ 74.0 eV is of particular interest. As discussed earlier, the aluminium in the Al–O–Si linkages refers to a peak at 74.1 eV. Thus, the possible assignment of this new peak is to the aluminium in the interfacial oxane bond bridging the PTS to the Al_2O_3. Such

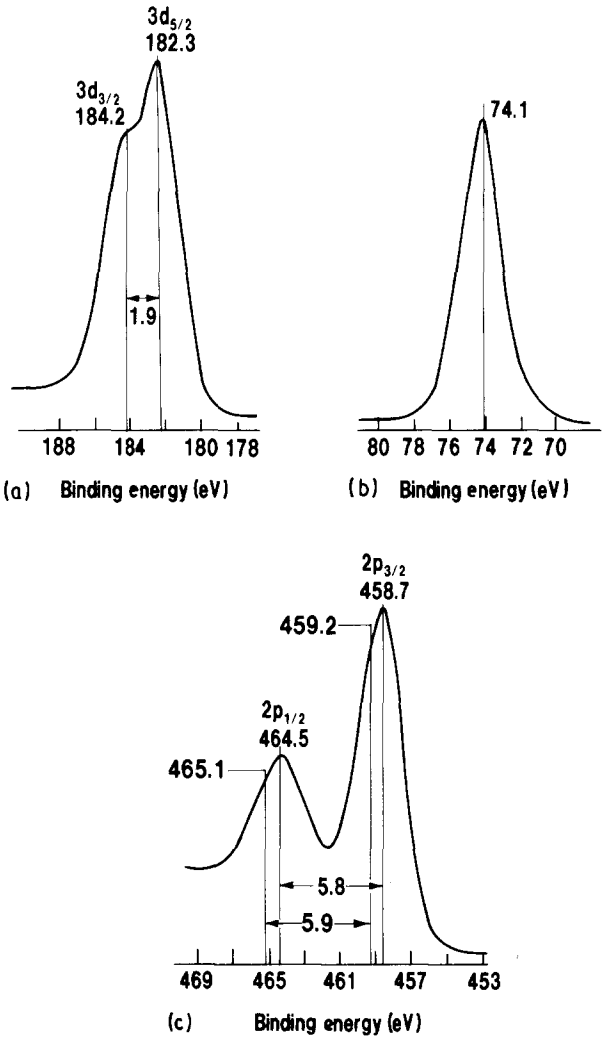

Figure 12 XPS spectra of (a) Zr 3d, (b) Al 2p, and (c) Ti 2p regions for PZS, PAS, and PTS coatings, respectively.

interfacial covalent bond structure may be illustrated as follows

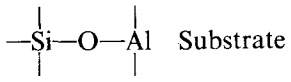

(II)

These covalent bonds presumably form through a dehydration–condensation reaction mechanism of the hydroxylated Al_2O_3 with the $\diagdown$Si–OH, in the PTS film. The investigations of the O 1s region appear to support the above-mentioned findings. The new peak at 531.2 eV, emerging at an interfacial boundary, (Fig. 14b) is associated with the oxygen in the Si–O–Al (on the surface of the substrate) bonds; whereas the position of the peak at 531.6 eV corresponds to the Al_2O_3 oxygen (Fig. 14a). The Si 2p signal (Fig. 15) is asymmetric because it consists of three components at 102.9, 101.7, and 99.6 eV. The major line at 101.7 eV can be ascribed to the Si in the M–O–Si linkages, and the weak shoulder at 102.9 eV to the Si in Si–O–Si linkages. The existence of other possible Si-based components could not be established on the basis of the minor peak at 99.6 eV. Apart from a slight broadening of the peak no special spectral features were observed on the Ti 2p doublet separation spectrum (Fig. 15) compared with that of PTS surface

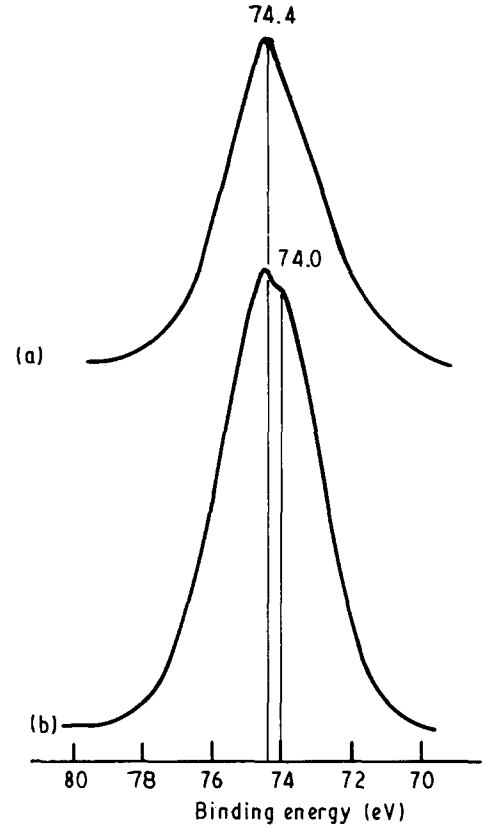

Figure 13 Al 2p spectra from (a) FPL-etched Al substrate surface and (b) critical interfacial zone between PTS and etched Al.

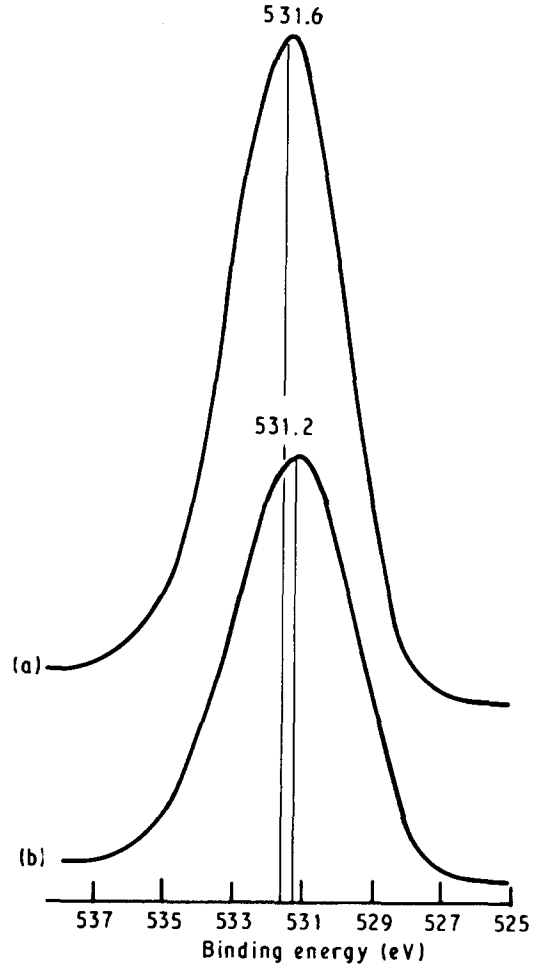

Figure 14 O 1s core level spectra for (a) etched Al surface and (b) PTS–Al interfacial area.

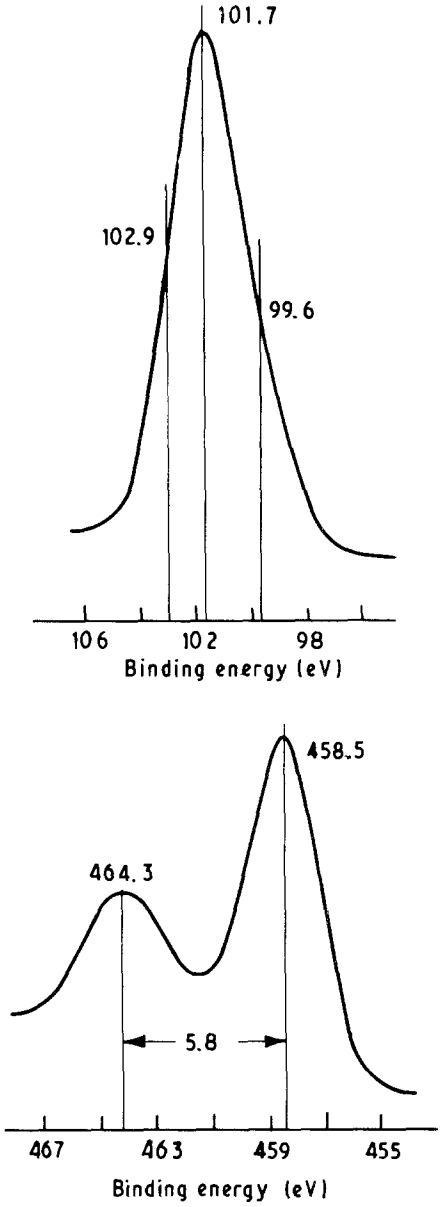

Figure 15 (a) Si 2p and (b) Ti 2p spectra from PTS/etched Al joint.

(Fig. 12). This information suggests that the extent of reactivity of titanium oxide, which acts as a cross-linking agent between the polysiloxane chains, with the Al_2O_3 is very small. Hence, the Al_2O_3 surface formed by FPL treatments of Al substrates preferentially links with the siloxane, rather than with the titanium oxide groups. From the above results, it can be rationalized that two major factors, (1) the cross-linking ability of metal oxides between the polysiloxane chains, and (2) the formation of PMS–Al interfacial chemical bonds, are responsible for greatly minimizing the development of stress cracks by shrinkage of pyrolysed PMS films. These important factors not only contribute to good film-forming behaviour, but also relate directly the affects of the corrosion protection of Al substrates.

All of the above data were correlated with corrosion protection provided by the pyrolysis-induced PMS coatings on FPL-etched Al. The corrosion data were obtained from the polarization curves for PMS-coated Al samples upon exposure in an aerated 0.5 M sodium chloride solution at 25 °C. The typical cathodic–anodic polarization curves exhibited a short Tafel region in the cathodic polarization, but no Tafel region was found at the anodic sites. To evaluate the protective performance of coatings, the corrosion potential, E_{corr}, and corrosion current, I_{corr}, were determined for the polarization curves. The former is defined as the potential at the transition point from cathodic to anodic polarization curves. I_{corr} values were measured by extrapolation of the cathodic Tafel slope. Table III summarizes these results. As seen in the table, the major affect of these PMS coatings on the corrosion protection of Al is to move the E_{corr} value to less negative potentials and to reduce the cathodic current, I_{corr}. In particular, the test samples coated with PTS produced significantly higher E_{corr} and lower I_{corr} values than compared with those for the uncoated samples (blanks). This strongly suggests that these PTS coating films will serve to provide good corrosion resistance to sodium chloride solution and in minimizing the corrosion rates of Al. The protective ability of other PMS systems seems to depend on the $TSPI/M(O_3H_7)_{4\text{ or }3}$ ratios in the precursor sol solution. Coatings derived from a higher ratio of 50/50 displace a lower corrosion resistance in sodium chloride medium. Similarly, the metal oxide–uncross-linked PS coating performed poorly and provided no significant corrosion resistance. The reason for the poor protection performance is, primarily, due to the presence of numerous microcracks and pits in the film layers. In other words, the sodium chloride solution penetrated the blemishes and progressively undermined the coatings.

TABLE III Corrosion potential, E_{corr}, and corrosion current, I_{corr}, values for PMS-coated and uncoated Al specimens

Coating systems ($TSPI/M(OC_3H_7)_{4\text{ or }3}$)	E_{corr} (v versus SCE)	I_{corr} (μA)
Uncoated (blank)	− 0.725	2.5
PS (100/0)	− 0.695	1.8
PZS (70/30)	− 0.625	7.8×10^{-1}
PZS (50/50)	− 0.710	1.5
PTS (70/30)	− 0.589	1.8×10^{-1}
PTS (50/50)	− 0.596	1.6×10^{-1}
PAS (70/30)	− 0.664	9.0×10^{-1}
PAS (50/50)	− 0.700	1.8

4. Conclusions

Inorganic amorphous polymetallosiloxane, PMS, can be synthesized through hydrolysis–polycondensation–pyrolysis reaction of sol-precursor solution systems consisting of *N*-[3-(triethoxysilyl)propyl]-4,5-dihydroimidazole (TSPI) and $M(OC_3H_7)_n$ (M = Zr, Ti and Al, $n = 3$ or 4) as a film-forming reagent, the HCl as a hydrolysis catalyst, and CH_3OH and water as a liquor medium. During this study of corrosion-protective thin films for low melting point Al substrates, the following seven items could be conclusively generalized as the major physico-chemical factors governing the film-forming behaviour of PMS under the sol precursor (25 °C) → sintering (150 °C) → annealing (350 °C) processes.

1. During the sol-film forming stage, the addition of HCl to the mixtures of TSPI and $M(OC_3H_7)_n$ induces the formation of hydroxylated metals, the Cl-substituted end groups in the monomeric organosilane and the separation of imidazole derivatives from TSPI.

2. In the sintering process of xerogel films at 150 °C, the formation of metal oxide polyorganosiloxane bond formed by the dechlorinating reaction between the Cl attached to propyl C in organosilane and the proton in the hydroxylated Zr or Ti compounds, played an important role in weight loss of the film.

3. Referring to item 2, the aluminium hydroxide, derived from $Al(OC_3H_7)_3$ in which the trivalent ion is the principal oxidation state, preferentially reacts with hydroxylated organosilane to form the Al–O–Si linkage at a low temperature. However, this linkage was broken when the sintered film was annealed at 350 °C, thereby creating large stress cracks and a high weight loss of the film.

4. The pyrolysis of titanium and zirconium oxides-incorporated polyorganosiloxane compounds led to the formation of titanium and zirconium oxides cross-linked with polysiloxane, while also eliminating carbonaceous groups and Cl compounds from the sintered materials. These cross-linked network structures served to minimize the development of stress cracks in the films pyrolysed at 350 °C.

5. Although a certain amount of crystalline anatase particles were present in the amorphous polytitanosiloxane (PTS) coatings, the moderate cross-linking effects of titanium oxides and the densification of the M–O–Si linkage provided the most effective coating film in this study.

6. The identification of covalent oxane bonds at the interfaces between the PTS and the FPL-etched Al substrate illustrates the possibility of strong adhesive forces.

7. Referring to items 4–6 described above, the integrated assignments of these factors were correlated directly to good corrosion resistance of Al alloys in the NaCl solution.

Acknowledgement

This work was performed under the auspices of the US Department of Energy, Washington, DC, under Contract no. DE-AC02-76CH00016, and supported by the US Army Research Office Program MIPR-AR0-102-89.

References

1. T. SUGAMA, L. E. KUKACKA and N. CARCIELLO, *Prog. Org. Coat.* **10** (1990) 173.
2. H. W. EICHNER and W. E. SCHOWALTER, Forest Products Laboratory Report no. 1813, Madison, WI (1950).
3. N. P. BANSAL, *J. Amer. Ceram. Soc.* **71** (1988) 666.
4. F. P. ENG and H. ISHIDA, *J. Mater. Sci.* **21** (1986) 1561.
5. C. N. R. RAO, "Chemical Applications of Infrared Spectroscopy" (Academic Press, New York, 1963) p. 323.
6. L. J. BELLAMY, "The Infrared Spectra of Complex Molecules" (Chapman and Hall, London, 1975) p. 318.
7. A. LEE SMITH, *Spectrochim. Acta* **16** (1960) 87.
8. D. H. R. BARTON, J. E. PGAE and C. W. SHOPPEE, *J. Chem. Soc.* (1956) 331.
9. N. V. SIDGWICK, "The Organic Chemistry of Nitrogen" (Clarendon Press, Oxford, 1966) p. 782.
10. R. A. SIMON, A. J. RICCO and M. S. WRIGHTON, *J. Amer. Chem. Soc.* **104** (1982) 2031.
11. G. RAMIS, P. QUINTARD, M. CAUCHATIER, G. BUSCA and V. LORENZELLI, *ibid.* **72** (1989) 1692.
12. S. W. LEE and R. A. CONDRATE Sr, *J. Mater. Sci.* **23** (1988) 2951.
13. B. E. YOLDAS, *ibid.* **14** (1979) 1843.
14. B. E. YOLDAS and D. P. PARTLOW, *ibid.* **23** (1988) 1895.
15. B. CARRIERE and J. P. DEVILLE, *J. Electron Spectrosc. Relat. Phenom.* **10** (1977) 85.
16. L. J. MATIENZO, *J. Adhes. Sci. Technol.* **3** (1989) 357.
17. T. E. MADEY, C. D. WAGNER and A. JOSHI, *J. Electron Spectrosc. Relat. Phenom.* **10** (1977) 359.
18. R. H. WEST and J. E. CASTLE, *Surf. Inter. Anal.* **4** (1982) 68.
19. R. CARACCIOLO and S. H. GAROFALIMI, *J. Amer. Ceram. Soc.* **71** (1988) C-346.
20. H. NASU, J. HEO and J. D. MACKENZIE, *J. Non-Cryst. Solids* **99** (1988) 140.
21. C. E. J. NICKERSON, C. ERNSBERGER, J. NICKERSON, A. E. MILLER and J. MOULDER, *J. Vac. Sci. Technol.* **6** (1985) 2415.
22. Y. W. KIM and J. G. LEE, *J. Amer. Ceram. Soc.* **72** (1989) 1333.
23. M. MURATA, K. WAKINO and S. IKEDA, *J. Elect. Spectros.* **6** (1975) 459.

Received 4 January
and accepted 19 November 1990